
Spin-Weighted Spherical CNNs

Carlos Esteves
GRASP Laboratory
University of Pennsylvania
machc@seas.upenn.edu

Ameesh Makadia
Google Research
makadia@google.com

Kostas Daniilidis
GRASP Laboratory
University of Pennsylvania
kostas@cis.upenn.edu

Abstract

Learning equivariant representations is a promising way to reduce sample and model complexity and improve the generalization performance of deep neural networks. The spherical CNNs are successful examples, producing $SO(3)$ -equivariant representations of spherical inputs. There are two main types of spherical CNNs. The first type lifts the inputs to functions on the rotation group $SO(3)$ and applies convolutions on the group, which are computationally expensive since $SO(3)$ has one extra dimension. The second type applies convolutions directly on the sphere, which are limited to zonal (isotropic) filters, and thus have limited expressivity. In this paper, we present a new type of spherical CNN that allows anisotropic filters in an efficient way, without ever leaving the spherical domain. The key idea is to consider spin-weighted spherical functions, which were introduced in physics in the study of gravitational waves. These are complex-valued functions on the sphere whose phases change upon rotation. We define a convolution between spin-weighted functions and build a CNN based on it. Experiments show that our method outperforms the isotropic spherical CNNs while still being much more efficient than using $SO(3)$ convolutions. The spin-weighted functions can also be interpreted as spherical vector fields, allowing applications to tasks where the inputs or outputs are vector fields.

1 Introduction

Learning representations from data enables a variety of applications that are not possible with other methods. Convolutional neural networks (CNNs) are powerful tools in representation learning, in great part due to their translation equivariance property that allows weight-sharing, exploiting the natural structure of audio, image, or video inputs.

Recently, there has been significant work extending equivariance to other groups of transformations [19, 11, 12, 43, 30, 16, 42, 39, 44, 17, 2] and designing equivariant CNNs on non-Euclidean domains [7, 15, 24, 36, 33, 10, 25, 36, 45]. Successful applications have been demonstrated in tasks such as 3D shape analysis [15, 17], medical imaging [41, 3], satellite/aerial imaging [12, 20], cosmology [12, 33], physics/chemistry [7, 24, 1]. Favorable results were also shown on popular upright natural image datasets such as CIFAR10/100 [38].

Rotation equivariant CNNs are the natural way to learn feature representations on spherical data. There are two prevailing designs, (a) convolution between spherical functions and zonal (isotropic; constant per latitude) filters [15], and (b) convolutions on $SO(3)$ after lifting spherical functions to the rotation group [7]. There is a clear distinction between these two designs: (a) is more efficient allowing to build representational capacity through deeper networks, and (b) has more expressive

We gratefully acknowledge support by the NSF TRIPODS 1934960 and the ONR N00014-17-1-2093 grants.

filters but is computationally expensive and thus is constrained to shallower networks. The question we consider in this paper is how do we achieve the expressivity/representation capacity of $\text{SO}(3)$ convolutions with the efficiency and scalability of spherical convolutions?

In this paper, we propose to leverage spin-weighted spherical functions (SWSFs), introduced by Newman and Penrose [32] in the study of gravitational waves. These are complex-valued functions on the sphere that, upon rotation, suffer a phase change besides the usual spherical translation. Our key observation is that a combination of SWSFs allows more expressive representations than scalar spherical functions, avoiding the need to lift features to the higher dimensional $\text{SO}(3)$. It also enables anisotropic filters, removing the filter constraint of purely spherical CNNs.

We define convolutions and cross-correlations of SWSFs. For bandlimited inputs, the operations can be computed exactly in the spectral domain, and are equivariant to the continuous group $\text{SO}(3)$. We build a CNN where filters and features are sets of SWSFs, and adapt nonlinearities, batch normalization, and pooling layers as necessary.

Besides more expressive and efficient representations, we can interpret the spin-weighted features as equivariant vector fields on the sphere, enabling applications where the inputs or outputs are vector fields. Current spherical CNNs [7, 15, 24, 33] cannot achieve equivariance in this sense, as illustrated in Fig. 1.

To evaluate vector field equivariance, we introduce a variation of MNIST where the images and their gradients are projected to the sphere. We propose three tasks on this dataset: 1) vector field classification, 2) vector field prediction from scalar fields, 3) scalar field prediction from vector fields.

To summarize our contributions,

1. We define the convolution and cross-correlation between sets of spin-weighted spherical functions. These are $\text{SO}(3)$ equivariant operations that respect the SWSFs properties.
2. We build a CNN based on these operations and adapt usual CNN components for sets of SWSFs as features and filters. This is, to the best of our knowledge, the first spherical CNN that operates on vector fields.
3. We demonstrate the efficacy of the spin-weighted spherical CNNs (SWSCNNs) in a variety of tasks including spherical image and vector field classification, predicting vector field from images and conversely.
4. We will make our code and datasets publicly available at <https://github.com/daniilidis-group/swscnn>.

2 Related work

Equivariant CNNs The first equivariant CNNs were applied to images on the plane [19, 12]. Cohen and Welling [11] formalize these models and name them group convolutional neural networks (G-CNNs). While initial methods were constrained to small discrete groups of rotations on the plane, they were later extended to larger groups [40], continuous rotations [43], rotations and scale [16], 3D rotations of voxel grids [44, 39], and point clouds [36].

Spherical CNNs G-CNNs can be extended to homogeneous spaces of groups of symmetries [26]; the quintessential example is the sphere S^2 as a homogeneous space of the group $\text{SO}(3)$, the setting of spherical CNNs. There are two main branches. The first branch, introduced by Cohen et al. [7], lifts the spherical inputs to functions on $\text{SO}(3)$, and its filters and features are functions on the group $\text{SO}(3)$, which is higher dimensional and thus more computationally expensive to process. Kondor

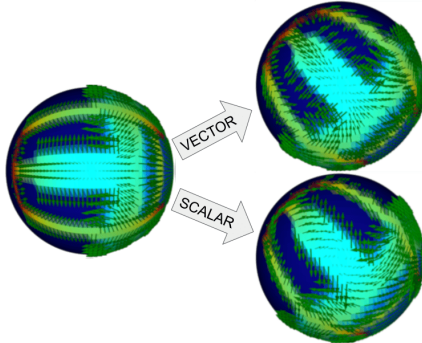


Figure 1: Each sphere shows a scalar and a vector field. Upon rotation, scalar fields transform by simply moving to another position, while vector fields must move and also rotate. Treating vector fields as scalar (bottom-right) results in incorrect behavior. The spin-weighted spherical CNNs equivariantly handle vector fields as inputs or outputs.

et al. [24] is another example. The second branch, introduced by Esteves et al. [15], is purely spherical and has filters and features on S^2 , using spherical convolution as the main operation. In this case, the filters are constrained to be zonal (isotropic), which limits the representational power. Perraudin et al. [33] also uses isotropic filters, but with graph convolutions instead of spherical convolutions.

Our approach lies between these two branches; it is not restricted to isotropic filters but it does not have to lift features to $\mathbf{SO}(3)$; we employ sets of SWSFs as filters and features.

Equivariant vector fields Our approach can equivariantly handle spherical vector fields as inputs or outputs. Marcos et al. [30] introduce a CNN on the plane whose features are vector fields obtained from rotated copies of filters. Cohen and Welling [8] formalize the concept of feature types that are vectors in a group representation space. This is extended to 3D Euclidean space by Weiler et al. [39]. Worrall et al. [43] introduce complex-valued features on \mathbb{R}^2 whose phases change upon rotation; this is similar in spirit to our method, but our features live on the sphere, requiring different machinery.

Cohen et al. [10] introduce a model that can theoretically produce vector field features on general manifolds. However, its current instantiation is only equivariant to the discrete group of rotations; in particular, each vector admits only six possible orientations. In contrast, our features are vector fields equivariant to the continuous group $\mathbf{SO}(3)$, thanks to the implementation in the spectral domain. Cohen et al. [9] allude to the possibility of building spherical CNNs that can process vector fields; we materialize these networks for the first time.

3 Background

In this section, we provide the mathematical background that guides our contributions. We first introduce the more commonly encountered spherical harmonics, then the generalization to the spin-weighted spherical harmonics (SWSHs). We also describe convolutions between spherical functions, which we will later generalize to convolutions between spin-weighted functions.

Spherical Harmonics The spherical harmonics $Y_m^\ell: S^2 \rightarrow \mathbb{C}$ form an orthonormal basis for the space $L^2(S^2)$ of square integrable functions on the sphere. Any function $f: S^2 \rightarrow \mathbb{C}$ in $L^2(S^2)$ can be decomposed in this basis via the spherical Fourier transform (SFT), and synthesized back exactly via its inverse,

$$\hat{f}_m^\ell = \int_{S^2} f(x) \overline{Y_m^\ell(x)} dx, \quad (1) \quad f(x) = \sum_{\ell=0}^{\infty} \sum_{|m| \leq \ell} \hat{f}_m^\ell Y_m^\ell(x). \quad (2)$$

We interchangeably use latitudes and longitudes (θ, ϕ) or points $x \in \mathbb{R}^3, \|x\| = 1$ to refer to the sphere. A function has bandwidth B when only components of order $\ell \leq B$ appear in the expansion.

The spherical harmonics are related to irreducible representations of the group $\mathbf{SO}(3)$ as follows,

$$D_{m,0}^\ell(\alpha, \beta, \gamma) = \sqrt{\frac{4\pi}{2\ell+1}} \overline{Y_m^\ell(\beta, \alpha)}, \quad (3)$$

where α, β and γ are ZYZ Euler angles and D^ℓ is a Wigner-D matrix. Since D^ℓ is a group representation and hence a group homomorphism, we obtain a rotation formula,

$$Y_m^\ell(gx) = \sum_{n=-\ell}^{\ell} \overline{D_{m,n}^\ell(g)} Y_n^\ell(x), \quad (4)$$

where we interchangeably use an element $g \in \mathbf{SO}(3)$ or Euler angles α, β and γ to refer to rotations.

Consider the rotation of a function represented by its coefficients by combining Eqs. (2) and (4),

$$f(gx) = \sum_{\ell=0}^{\infty} \sum_{n=-\ell}^{\ell} \left(\sum_{m=-\ell}^{\ell} \hat{f}_m^\ell \overline{D_{m,n}^\ell(g)} \right) Y_n^\ell(x). \quad (5)$$

This shows that when $f(x) \mapsto f(gx)$, the coefficients transform as

$$\hat{f}_n^\ell \mapsto \sum_m \overline{D_{m,n}^\ell(g)} \hat{f}_m^\ell \quad (6)$$

Finally, we recall how convolutions and cross-correlations of spherical functions are computed in the spectral domain. Esteves et al. [15] define the convolution between two spherical functions as Eq. (7) while Makadia and Daniilidis [29] and Cohen et al. [7] define the spherical cross-correlation as Eq. (8),

$$(\widehat{k * f})_m^\ell = 2\pi \sqrt{\frac{4\pi}{2\ell + 1}} \hat{f}_m^\ell \hat{k}_0^\ell, \quad (7) \quad (\widehat{k \star f})_{m,n}^\ell = \hat{f}_m^\ell \overline{\hat{k}_n^\ell}, \quad (8)$$

Both are shown to be equivariant through Eq. (6). The left-hand side of Eq. (7) correspond to the Fourier coefficients of a spherical function, while the left-hand side of Eq. (8) correspond to the Fourier coefficients of a function on $\mathbf{SO}(3)$.

This section laid the foundation for the spin-weighted generalization. We refer to Esteves [14] for a longer exposition on this topic and to Vilenkin and Klimyk [37] and Folland [18] for the full details.

Spin-Weighted Spherical Harmonics The spin-weighted spherical functions (SWSFs) are complex-valued functions on the sphere whose phases change upon rotation. They have different types determined by the spin weight.

Let ${}_s f: S^2 \rightarrow \mathbb{C}$ be a SWSF with spin weight s , λ_α a rotation by α around the polar axis, and ν the north pole. In a conventional spherical function, ν is fixed by the rotation, so $(\lambda_\alpha(f))(\nu) = f(\nu)$. In a spin-weighted function, however, the rotation results in a phase change,

$$(\lambda_\alpha({}_s f))(\nu) = {}_s f(\nu) e^{-is\alpha}. \quad (9)$$

If the spin weight is $s = 0$, this is equivalent to the conventional spherical functions.

The spin-weighted spherical harmonics (SWSHs) form a basis of the space of square-integrable spin-weighted spherical functions; for all square-integrable ${}_s f$, we can write

$${}_s f(\theta, \phi) = \sum_{\ell \in \mathbb{N}} \sum_{m=-\ell}^{\ell} {}_s Y_m^\ell(\theta, \phi) \hat{f}_m^\ell, \quad (10)$$

where \hat{f}_m^ℓ are the expansion coefficients, and the decomposition is defined similarly to Eq. (1). For $s = 0$, the SWSHs are exactly the spherical harmonics; we have ${}_0 Y_m^\ell = Y_m^\ell$.

The SWSHs are related to the matrix elements D_{mn}^ℓ of $\mathbf{SO}(3)$ representations as follows,

$$D_{m,-s}^\ell(\alpha, \beta, \gamma) = (-1)^s \sqrt{\frac{4\pi}{2\ell + 1}} \overline{{}_s Y_m^\ell(\beta, \alpha)} e^{-is\gamma}. \quad (11)$$

Note how different spin-weights are related to different columns of D^ℓ , while the standard spherical harmonics are related to a single column as in Eq. (3). This shows that the SWSHs can be seen as functions on $\mathbf{SO}(3)$ with sparse spectrum, a point of view that is advocated by Boyle [5].

The SWSHs do not transform among themselves upon rotation as the spherical harmonics (Eq. (4)) due to the extra phase change. Fortunately, the coefficients of expansion of a SWSF into the SWSHs do transform among themselves according to Eq. (6). When ${}_s f(x) \mapsto {}_s f(gx)$,

$${}_s \hat{f}_n^\ell \mapsto \sum_m \overline{D_{m,n}^\ell(g)} {}_s \hat{f}_m^\ell. \quad (12)$$

This is crucial for defining equivariant convolutions between combinations of SWSFs as we will do in Section 4.1. We refer to Castillo [6] and Boyle [4, 5] for more details regarding SWSFs.

4 Method

We introduce a fully convolutional network, the spin-weighted spherical CNN (SWSCNN), where layers are based on spin-weighted convolutions, and filters and features are combinations of SWSFs. We define spin-weighted convolutions and cross-correlations, show how to efficiently implement them, and adapt common neural network layers to work with combinations of SWSFs.

4.1 Spin-Weighted Convolutions and Correlations

We define and evaluate the convolutions and cross-correlations in the spectral domain. Consider a set of spin weights W_F, W_K and sets of functions $F = \{{}_s f: S^2 \rightarrow \mathbb{C} \mid s \in W_F\}$ and filters $K = \{{}_s k: S^2 \rightarrow \mathbb{C} \mid s \in W_K\}$ to be convolved.

Spin-weighted convolution We define the convolution between F and K as follows,

$${}_s(\widehat{F * K})_m^\ell = \sum_{i \in W_F} \hat{f}_m^\ell \hat{k}_i^\ell, \quad (13)$$

where $s \in W_K$ and $-\ell \leq m \leq \ell$. Only coefficients ${}_s \hat{k}_i^\ell$ where $i \in W_F$ influence the output, imposing sparsity in the spectra of K . The convolution $F * K$ is also a set of SWSFs with $s \in W_K$, the same spin weights as K ; we leverage this to specify the desired sets of spins at each layer.

Application of the rotation formula in Eq. (12) shows the $\mathbf{SO}(3)$ equivariance of this operation. Let λ_g be the rotation operator describing Eq. (12). We have,

$$\begin{aligned} \sum_{i \in W_F} \lambda_g({}_i \hat{f}_n^\ell) {}_s \hat{k}_i^\ell &= \sum_{i \in W_F} \sum_m \overline{D_{m,n}^\ell(g)} {}_i \hat{f}_m^\ell {}_s \hat{k}_i^\ell \\ &= \sum_m \overline{D_{m,n}^\ell(g)} \sum_{i \in W_F} {}_i \hat{f}_m^\ell {}_s \hat{k}_i^\ell \\ &= \sum_m \overline{D_{m,n}^\ell(g)} {}_s (\widehat{F * K})_m^\ell \\ &= \lambda_g({}_s (\widehat{F * K})_n^\ell). \end{aligned} \quad (14)$$

Now consider the spherical convolution defined in Eq. (7). It follows immediately that it is, up to a constant, a special case of the spin-weighted convolution, where F and K have only one element with $s = 0$, and only the filter coefficients of form ${}_0 \hat{k}_0^\ell$ are used.

Spin-weighted cross-correlation We define the cross-correlation between F and K as follows,

$${}_s(\widehat{F \star K})_m^\ell = \sum_{i \in W_F \cap W_K} \hat{f}_m^\ell \overline{\hat{k}_s^\ell}, \quad (16)$$

In this case, only the spins that are common to F and K are used, but all spins may appear in the output, so it can be seen as a function on $\mathbf{SO}(3)$ with dense spectrum. To ensure a desired set of spins in $F \star K$, we can sparsify the spectra in K by eliminating some orders. A procedure similar to Eq. (15) proves the $\mathbf{SO}(3)$ equivariance of this operation.

The spin-weighted cross-correlation generalizes the spherical cross-correlation. When F and K contain only a single spin weight $s = 0$, the summation in Eq. (16) will contain only one term and we recover the spherical cross-correlation defined in Eq. (8).

Examples To visualize the convolution and cross-correlations, we use the phase of the complex numbers and local frames to obtain a vector field. We visualize combinations of SWSFs by associating pixel intensities with the spin-weight $s = 0$ and plotting vectors fields for each $s > 0$.

Consider an input $F = \{{}_0 f, {}_1 f\}$ and filter $K = \{{}_0 k, {}_1 k\}$, both with spin weights 0 and 1. Their convolution also has spins 0 and 1, as shown on the left side of Fig. 2. Now consider a scalar valued (spin $s = 0$) input $F = \{{}_0 f\}$ and filter $K = \{{}_0 k\}$. The cross-correlation will have components of every spin, but we only take spin weights 0 and 1 to visualize (this is equivalent to eliminating all orders larger than 1 in the spectrum of k); Fig. 2 shows the results.

4.2 Architecture

Our main operation is the convolution defined in Section 4.1. Since components with the same spin can be added, the generalization to multiple channels is immediate. The convolution combines features of different spins, so we enforce the same number of channels per spin per layer. Each feature map then consists of a set of SWSFs of different spins, $F = \{{}_s f : S^2 \rightarrow \mathbb{C}^k \mid s \in W_F\}$, where k is the number of channels and W_F the set of spin weights.

Filter localization We compute the convolutions in the spectral domain but apply nonlinearities, batch normalization and pooling in the spatial domain. This requires expanding the feature maps into the SWSFs basis and back at every layer, but the filters themselves are parameterized by

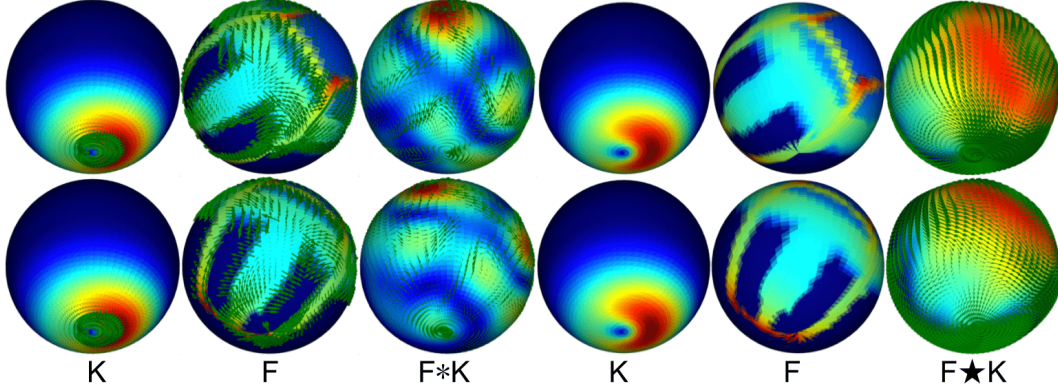


Figure 2: Left block (2×3): convolution between combinations of functions of spin weights $s = 0$ and $s = 1$. The operation is equivariant as a vector field and outputs carry the same spin-weights. Right block (2×3): spin-weighted cross-correlation between scalar spherical functions. The operation is also equivariant as a vector field and we show the outputs corresponding to spins 0 and 1.

their spectrum. We follow the idea of Esteves et al. [15] to enforce filter localization with spectral smoothness. Their filters are of the form ${}_0\hat{k}_0^\ell$, so the spectrum lies on a line and can be interpolated from a few anchor points, smoothing it out and reducing the number of parameters. In our case, the filters take the general form ${}_s\hat{k}_m^\ell$ where $s \in W_{F*K}$ are the output spin weights and $m \in W_F$ are the input spin weights. We then interpolate the spectrum of each component along the degrees ℓ , resulting in a factor of $|W_{F*K}| |W_F|$ more parameters per layer.

Batch normalization and nonlinearity We force features with spin weight $s = 0$ to be real by taking their real part after every convolution, allowing the use of the common rectified linear unit (ReLU) as the nonlinearity and the standard batch normalization from Ioffe and Szegedy [22].

For $s > 0$, we have complex-valued feature maps. We employ a combination of batch normalization and nonlinearity applied only on the magnitudes. Let ${}_s f$ be a feature with $s > 0$ and β the batch normalization operator. We apply the following operation after each convolution, which serves as batch normalization and nonlinearity, where the max, magnitude, and multiplication are pointwise,

$${}_s f \mapsto {}_s f \max(\beta(|{}_s f|), 0). \quad (17)$$

Complexity analysis We follow Hufnberger and Wandelt [21] for the spin-weighted spherical Fourier transform (SWSFT) implementation (see appendix for details), whose complexity for bandwidth B is $\mathcal{O}(B^3)$. While it is asymptotically slower than the $\mathcal{O}(B^2 \log^2 B)$ of the standard SFT from Driscoll and Healy [13], the difference is small for bandwidths typically needed in practice [7, 15, 24]. The rotation group Fourier transform (SOFT) implementation from Kostelec and Rockmore [27] is $\mathcal{O}(B^4)$. Our final model requires $|W|$ transforms per layer, so it is asymptotically a factor $|W|^{B/\log^2 B}$ slower than using SFT as in Esteves et al. [15], and a factor $B/|W|$ faster than using the SOFT as in Cohen et al. [7]. Typical values in our experiments are $B = 32$ and $|W| = 2$.

5 Experiments

We show experiments on image and vector field classification, image prediction from a vector field, and vector field prediction from an image, where all images and vector fields are on the sphere.

We use spin weights 0 and 1 in all experiments. When inputs do not have both spins, the first layer is designed such that its outputs have. All following layers and filters also have spins 0 and 1.

Every model is trained with different random seeds five times and averages and standard deviations (within parenthesis) are reported. See the appendix for training procedure details.

5.1 Spherical Image Classification

Our first experiment is on the Spherical MNIST dataset introduced by Cohen et al. [7]. This is an image classification task where the handwritten digits from MNIST are projected on the sphere. Three modes are evaluated depending on whether the training/test set are rotated. For example, in mode NR/R, the training set is not rotated and the test set is.

We follow the network topology from Esteves et al. [15], switching from spherical convolutions to spin-weighted convolutions, and adapting the numbers of channels and parameters per filter to have the same total parameter count. Table 1 shows the results; we outperform previous equivariant spherical CNNs in every mode.

Table 1: Spherical MNIST results. Our model is more expressive than the isotropic and more efficient than the previous anisotropic spherical CNNs, allowing deeper models and improved performance.

	NR/NR	R/R	NR/R	params
Planar CNN	99.07(4)	81.07(63)	17.23(71)	59k
Cohen et al. [7]	95.59	94.62	93.40	58k
Kondor et al. [24]	96.40	96.60	96.00	-
Esteves et al. [15]	98.75(8)	98.71(5)	98.08(24)	57k
Ours	99.37(5)	99.37(1)	99.08(12)	58k

5.2 Spherical Vector Field Classification

One crucial advantage of the SWSCNNs is that they are equivariant as vector fields. To demonstrate this, we introduce a spherical vector field dataset. As usual, we take MNIST as the source. We construct the vectors as image gradients using Sobel kernels, then project them into the sphere. To make the problem more challenging, we follow Larochelle et al. [28] and swap the train and test sets so there are 10k images for training and 50k for test. We call this dataset the spherical vector field MNIST (SVFMNIST).

The vector field is converted to a spin weight $s = 1$ complex-valued spherical function using a predefined local tangent frame per point on the sphere. A similar procedure allows to convert $s = 1$ features to output vector fields.

The first task we consider is classification. We use the same architecture as in the previous experiment, the only difference is that now the first layer maps from spin 1 to spins 0 and 1. Table 2 shows the results. The planar and spherical CNN models take the vector field as a 2-channel input. The NR/R column clearly shows the advantage of vector field equivariance; the baselines cannot generalize to unseen vector field rotations, even when they are equivariant in the scalar sense as [15].

Table 2: Spherical vector field MNIST classification results. When vector field equivariance is required, the gap between our method and the spherical and planar baselines is even larger.

	NR/NR	R/R	NR/R
Planar	97.7(2)	50.0(8)	14.6(9)
[15]	98.4(1)	94.5(5)	24.8(8)
Ours	98.2(1)	97.8(2)	98.2(7)

5.3 Spherical Vector Field Prediction

The SWSCNNs can also be used for dense prediction. We introduce two new tasks on SVFMNIST, 1) predicting a vector field from an image and 2) predicting an image from a vector field. For these tasks, we implement a fully convolutional U-Net architecture [35] with spin-weighted convolutions.

When the image is the grayscale digit and the vector field comes from the gradients, both tasks can be easily solved via discrete integration and differentiation. We call this case “easy” and show it on the left side of table Table 3. It highlights a limitation of isotropic spherical CNNs; the results show that the constrained filters cannot approximate a simple image gradient operator.

We also experiment with a more challenging scenario, where the digits are colored and the vector fields are rotated based on the digit category. These are semantic tasks that require the network to implicitly classify the input in order to correctly predict output color and vector directions.

Table 3 shows the results. While the planar baseline does well in the “easy” tasks that can be solved with simple linear operators, our model still outperforms it when generalization to unseen rotations is demanded (NR/R). In the “hard”, task the SWSCNNs are clearly superior by large margins. We show sample inputs and outputs in Fig. 3; see the appendix for more.

Table 3: Vector field to image and image to vector field results on SVFMNIST. The SWSCNNs show superior performance especially on the more challenging tasks. The metric is the mean-squared error $\times 10^3$ (lower is better). All models have around 112k parameters.

	easy			hard		
	NR/NR	R/R	NR/R	NR/NR	R/R	NR/R
Image to Vector Field						
Planar	0.3(1)	5.0(1)	9.3(1)	16.9(5)	26.0(1)	32.9(2)
Esteves et al. [15]	9.7(3)	31.0(2)	45.6(7)	13.3(6)	28.5(4)	41.6(4)
Ours	2.9(2)	3.4(1)	4.3(1)	11.6(6)	9.2(4)	10.2(6)
Vector Field to Image						
Planar	1.4(1)	3.2(1)	6.9(4)	3.3(2)	13.4(2)	21.1(3)
Esteves et al. [15]	3.8(1)	4.9(2)	15(2)	2.6(1)	6.4(2)	20.3(9)
Ours	3.5(1)	3.8(1)	4.0(1)	2.6(1)	2.7(1)	2.9(1)

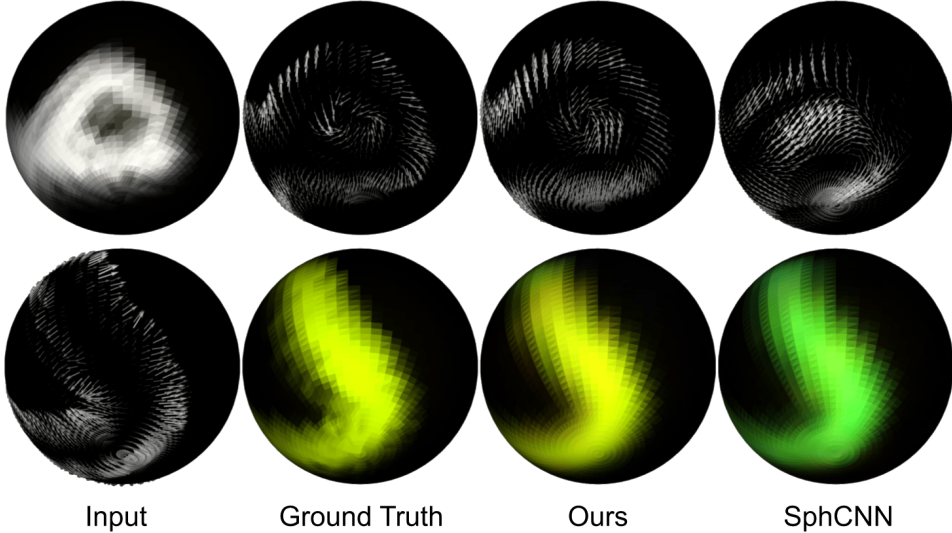


Figure 3: Inputs and outputs, R/R. **Top:** image to vector field. Our method predicts the position and orientation of each vector correctly, while the spherical CNN [15] cannot. **Bottom:** vector field to image. Here the spherical CNN predicts the incorrect color while the SWSCNNs have no problem.

6 Conclusion

In this paper, we introduced the spin-weighted spherical CNNs, which use sets of spin-weighted spherical functions as features and filters, and employ layers of a newly introduced spin-weighted spherical convolution to process spherical images or spherical vector fields. Our model achieves superior performance on the tasks attempted, at a reasonable computational cost. We foresee applications of the SWSCNNs to 3D shape analysis, climate/atmospheric data analysis and other tasks where inputs or outputs can be represented as spherical images or vector fields.

References

- [1] Brandon M. Anderson, Truong-Son Hy, and Risi Kondor. “Cormorant: Covariant Molecular Neural Networks”. In: *Advances in Neural Information Processing Systems 32: Annual Conference on Neural Information Processing Systems 2019, NeurIPS 2019*. 2019, pp. 14510–14519.
- [2] Erik J. Bekkers. “B-Spline CNNs on Lie groups”. In: *8th International Conference on Learning Representations, ICLR 2020*. 2020.
- [3] Erik J Bekkers, Maxime W Lafarge, Mitko Veta, Koen AJ Eppenhof, Josien PW Pluim, and Remco Duits. “Roto-translation covariant convolutional networks for medical image analysis”. In: *International Conference on Medical Image Computing and Computer-Assisted Intervention*. Springer. 2018, pp. 440–448.
- [4] Michael Boyle. “Angular velocity of gravitational radiation from precessing binaries and the corotating frame”. In: *Physical Review D* 87.10 (2013), p. 104006.
- [5] Michael Boyle. “How should spin-weighted spherical functions be defined?” In: *Journal of Mathematical Physics* 57.9 (Sept. 2016), p. 092504. ISSN: 1089-7658. DOI: [10.1063/1.4962723](https://doi.org/10.1063/1.4962723). URL: <http://dx.doi.org/10.1063/1.4962723>.
- [6] Gerardo F Torres del Castillo. *3-D spinors, spin-weighted functions and their applications*. Vol. 32. Springer Science & Business Media, 2012.
- [7] Taco S. Cohen, Mario Geiger, Jonas Köhler, and Max Welling. “Spherical CNNs”. In: *International Conference on Learning Representations*. 2018. URL: <https://openreview.net/forum?id=Hkxbd5xZRb>.
- [8] Taco S. Cohen and Max Welling. “Steerable CNNs”. In: *5th International Conference on Learning Representations, ICLR 2017*. 2017.
- [9] Taco S Cohen, Mario Geiger, and Maurice Weiler. “A General Theory of Equivariant CNNs on Homogeneous Spaces”. In: *Advances in Neural Information Processing Systems*. 2019, pp. 9142–9153.
- [10] Taco Cohen, Maurice Weiler, Berkay Kicanaoglu, and Max Welling. “Gauge Equivariant Convolutional Networks and the Icosahedral CNN”. In: *Proceedings of the 36th International Conference on Machine Learning, ICML 2019*. 2019.
- [11] Taco Cohen and Max Welling. “Group equivariant convolutional networks”. In: *International conference on machine learning*. 2016, pp. 2990–2999.
- [12] Sander Dieleman, Jeffrey De Fauw, and Koray Kavukcuoglu. “Exploiting Cyclic Symmetry in Convolutional Neural Networks”. In: *Proceedings of the 33rd International Conference on Machine Learning, ICML 2016*. 2016, pp. 1889–1898.
- [13] James R Driscoll and Dennis M Healy. “Computing Fourier transforms and convolutions on the 2-sphere”. In: *Advances in applied mathematics* 15.2 (1994), pp. 202–250.
- [14] Carlos Esteves. “Theoretical Aspects of Group Equivariant Neural Networks”. In: *CoRR* abs/2004.05154 (2020). arXiv: [2004.05154](https://arxiv.org/abs/2004.05154).
- [15] Carlos Esteves, Christine Allen-Blanchette, Ameesh Makadia, and Kostas Daniilidis. “Learning SO(3) Equivariant Representations with Spherical CNNs”. In: *The European Conference on Computer Vision (ECCV)*. Sept. 2018.
- [16] Carlos Esteves, Christine Allen-Blanchette, Xiaowei Zhou, and Kostas Daniilidis. “Polar Transformer Networks”. In: *6th International Conference on Learning Representations, ICLR 2018*. 2018.
- [17] Carlos Esteves, Yinshuang Xu, Christine Allen-Blanchette, and Kostas Daniilidis. “Equivariant Multi-View Networks”. In: *The IEEE International Conference on Computer Vision (ICCV)*. Oct. 2019.
- [18] Gerald B Folland. *A course in abstract harmonic analysis*. Chapman and Hall/CRC, 2016.
- [19] Robert Gens and Pedro M Domingos. “Deep symmetry networks”. In: *Advances in neural information processing systems*. 2014, pp. 2537–2545.
- [20] Joao F Henriques and Andrea Vedaldi. “Warped convolutions: Efficient invariance to spatial transformations”. In: *Proceedings of the 34th International Conference on Machine Learning-Volume 70*. JMLR. org. 2017, pp. 1461–1469.
- [21] Kevin M. Huffenberger and Benjamin D. Wandelt. “Fast and Exact Spin-s Spherical Harmonic Transforms”. In: *The Astrophysical Journal Supplement Series* 189.2 (July 2010), pp. 255–260. DOI: [10.1088/0067-0049/189/2/255](https://doi.org/10.1088/0067-0049/189/2/255).

- [22] Sergey Ioffe and Christian Szegedy. “Batch Normalization: Accelerating Deep Network Training by Reducing Internal Covariate Shift”. In: *Proceedings of the 32nd International Conference on Machine Learning*. 2015, pp. 448–456.
- [23] Diederik P. Kingma and Jimmy Ba. “Adam: A Method for Stochastic Optimization”. In: *3rd International Conference on Learning Representations, ICLR 2015*. 2015. URL: <http://arxiv.org/abs/1412.6980>.
- [24] Risi Kondor, Zhen Lin, and Shubhendu Trivedi. “Clebsch–gordan nets: a fully fourier space spherical convolutional neural network”. In: *Advances in Neural Information Processing Systems*. 2018, pp. 10138–10147.
- [25] Risi Kondor, Hy Truong Son, Horace Pan, Brandon M. Anderson, and Shubhendu Trivedi. “Covariant Compositional Networks For Learning Graphs”. In: *6th International Conference on Learning Representations, ICLR 2018, Vancouver, BC, Canada, April 30 - May 3, 2018, Workshop Track Proceedings*. 2018.
- [26] Risi Kondor and Shubhendu Trivedi. “On the Generalization of Equivariance and Convolution in Neural Networks to the Action of Compact Groups”. In: *International Conference on Machine Learning, ICML*. 2018.
- [27] Peter J Kostelec and Daniel N Rockmore. “FFTs on the rotation group”. In: *Journal of Fourier Analysis and Applications* 14.2 (2008), pp. 145–179.
- [28] Hugo Larochelle, Dumitru Erhan, Aaron Courville, James Bergstra, and Yoshua Bengio. “An empirical evaluation of deep architectures on problems with many factors of variation”. In: *Proceedings of the 24th international conference on Machine learning*. ACM. 2007, pp. 473–480.
- [29] A. Makadia and K. Daniilidis. “Rotation recovery from spherical images without correspondences”. In: *IEEE Transactions on Pattern Analysis and Machine Intelligence* 28.7 (July 2006), pp. 1170–1175. ISSN: 0162-8828. DOI: [10.1109/TPAMI.2006.150](https://doi.org/10.1109/TPAMI.2006.150).
- [30] Diego Marcos, Michele Volpi, Nikos Komodakis, and Devis Tuia. “Rotation Equivariant Vector Field Networks”. In: *IEEE International Conference on Computer Vision, ICCV 2017*. 2017, pp. 5058–5067.
- [31] Jason D McEwen. “Fast, exact (but unstable) spin spherical harmonic transforms”. In: *arXiv preprint arXiv:0807.4494* (2008).
- [32] Ezra T Newman and Roger Penrose. “Note on the Bondi-Metzner-Sachs Group”. In: *Journal of Mathematical Physics* 7.5 (1966), pp. 863–870.
- [33] Nathanaël Perraudin, Michaël Defferrard, Tomasz Kacprzak, and Raphael Sgier. “DeepSphere: Efficient spherical convolutional neural network with HEALPix sampling for cosmological applications”. In: *Astronomy and Computing* 27 (2019), pp. 130–146.
- [34] Torben Risbo. “Fourier transform summation of Legendre series and D-functions”. In: *Journal of Geodesy* 70.7 (1996), pp. 383–396.
- [35] Olaf Ronneberger, Philipp Fischer, and Thomas Brox. “U-Net: Convolutional Networks for Biomedical Image Segmentation”. In: *International Conference on Medical Image Computing and Computer Assisted Intervention (MICCAI)*. 2015.
- [36] Nathaniel Thomas, Tess Smidt, Steven Kearnes, Lusann Yang, Li Li, Kai Kohlhoff, and Patrick Riley. “Tensor Field Networks: Rotation-and Translation-Equivariant Neural Networks for 3D Point Clouds”. In: *arXiv preprint arXiv:1802.08219* (2018).
- [37] N. Ja. Vilenkin and A. U. Klimyk. *Representation of Lie Groups and Special Functions*. Springer Netherlands, 1991.
- [38] Maurice Weiler and Gabriele Cesa. “General E(2)-Equivariant Steerable CNNs”. In: *Advances in Neural Information Processing Systems*. 2019, pp. 14334–14345.
- [39] Maurice Weiler, Mario Geiger, Max Welling, Wouter Boomsma, and Taco Cohen. “3D Steerable CNNs: Learning Rotationally Equivariant Features in Volumetric Data”. In: *Advances in Neural Information Processing Systems*. Ed. by S. Bengio, H. Wallach, H. Larochelle, K. Grauman, N. Cesa-Bianchi, and R. Garnett. 2018.
- [40] Maurice Weiler, Fred A. Hamprecht, and Martin Storath. “Learning Steerable Filters for Rotation Equivariant CNNs”. In: *2018 IEEE Conference on Computer Vision and Pattern Recognition, CVPR 2018*. 2018, pp. 849–858.
- [41] Marysia Winkels and Taco S Cohen. “3D G-CNNs for Pulmonary Nodule Detection”. In: *arXiv preprint arXiv:1804.04656* (2018).

- [42] Daniel E. Worrall and Max Welling. “Deep Scale-spaces: Equivariance Over Scale”. In: *Advances in Neural Information Processing Systems 32: Annual Conference on Neural Information Processing Systems 2019, NeurIPS 2019*. 2019, pp. 7364–7376.
- [43] Daniel E Worrall, Stephan J Garbin, Daniyar Turmukhambetov, and Gabriel J Brostow. “Harmonic networks: Deep translation and rotation equivariance”. In: *Proc. IEEE Conf. on Computer Vision and Pattern Recognition (CVPR)*. Vol. 2. 2017.
- [44] Daniel Worrall and Gabriel Brostow. “Cubenet: Equivariance to 3d rotation and translation”. In: *Proceedings of the European Conference on Computer Vision (ECCV)*. 2018, pp. 567–584.
- [45] Yongheng Zhao, Tolga Birdal, Jan Eric Lenssen, Emanuele Menegatti, Leonidas Guibas, and Federico Tombari. “Quaternion Equivariant Capsule Networks for 3d Point Clouds”. In: *CoRR* (2019). arXiv: [1912.12098](https://arxiv.org/abs/1912.12098) [[cs.LG](#)].

Appendices

A Introduction

In this supplementary material we give more details about the datasets in Appendix B, about the experiments in Appendix C, and we describe the SWSH transform implementation in Appendix D.

B Datasets

We show samples of the SVFMNIST dataset in Fig. 4. This is the dataset used in the vector field classification task.

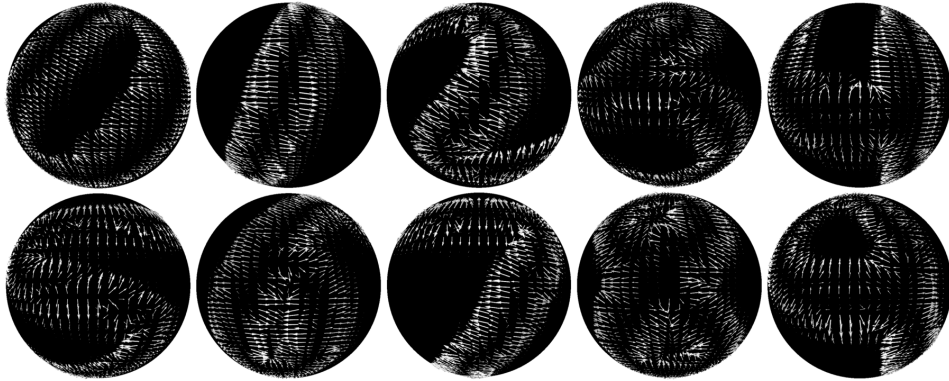


Figure 4: Samples from SVFMNIST, classification task. We show one sample for each category in canonical orientation for easy visualization.

For the dense prediction tasks, we introduce modifications in the targets to make them more challenging. When predicting an image from a vector field, we introduce color in the output based on the target category. We determine the color in HSV space, where the value is the original grayscale value, the hue is $c/10$ for category c , and the saturation is set to one. The target is then converted back to RGB. Figure 5 shows a few input/target pairs.

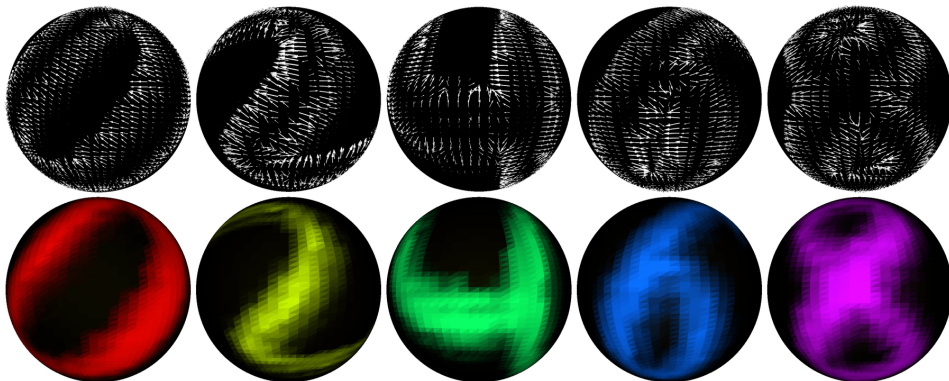


Figure 5: Samples from SVFMNIST, image from vector field prediction task. Top shows input vector fields, bottom the target spherical images. Note that the targets have different colors based on the category, so the task cannot be solved via simple gradient integration. Samples are in canonical orientation for easy visualization.

When predicting a vector field from an image, we introduce an angular offset on all vectors that depends on the target category. The offset for category c is given by $\exp 2\pi ic/10$. Figure 6 shows a few input/target pairs.

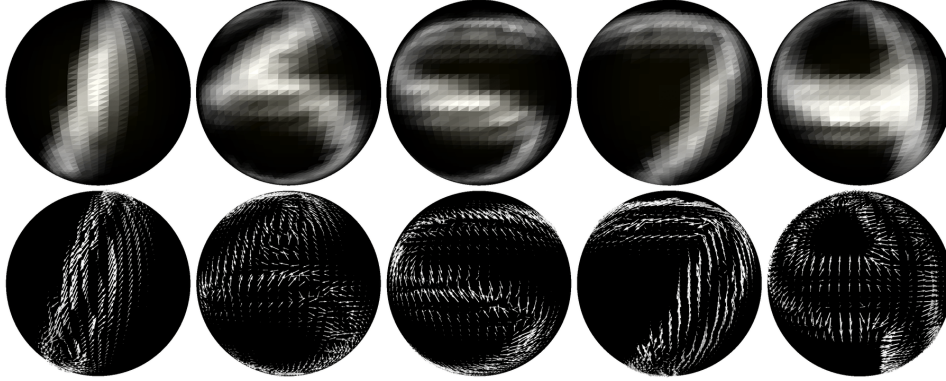


Figure 6: Samples from SVFMNIST, vector field from image prediction task. Top shows input spherical images, bottom the target vector fields. The targets have different angular offsets based on the category so the task cannot be solved via simple image gradient estimation. Samples are in canonical orientation for easy visualization.

C Experiments details

C.1 Training

In all experiments, we train for 12 epochs using the Adam optimizer [23]. We set the initial learning rate to 1×10^{-3} and decay it to 2×10^{-4} epoch 6 and 4×10^{-5} at epoch 10. The mini-batch size is set to 32 and input resolution is 64×64 .

The usual cross-entropy loss is optimized for the classification experiments, and the mean square error is minimized for dense prediction.

C.2 Architectures

Classification The architectures for spherical image and vector field classification are the same.

The spherical baseline follows Esteves et al. [15], with spherical convolutions, six layers with 16, 16, 32, 32, 58, 58 channels per layer, and 8 filter parameters per layer.

We follow the same general topology, switching from spherical to spin-weighted convolutions. Since our filters have richer spectra, they need more parameters. In order to keep similar number of parameters between competing models, we set the number parameters per spin-order pair (s, m) to 6, 6, 4, 4, 3, 3 at each layer. We also cut the number of channels per layer, so while we have the same number of parameters, we have significantly fewer feature maps. The final architecture has 16, 16, 20, 24, 28, 32 channels per layer, with pooling every two layers, and our custom batch normalization applied at every layer.

The planar baseline has the same number of layers and uses 2D convolutions with 3×3 kernels. We set the number of channels per layer to 16, 16, 32, 32, 54, 54. to match the number of parameters of the other models.

Spherical vector field/image prediction We design a different architecture for dense prediction, which is essentially a fully convolutional U-Net [35] with spin-weighted convolutions.

We use 16, 32, 32, 32, 32, 16 channels per layer, with pooling in the first two layers and nearest neighbors upsampling in the last two. The number of filter parameters chosen per spin-order per layer is 6, 4, 3, 3, 4, 6.

The spherical CNN baseline uses spherical convolutions and sets the numbers of filter parameters to 8 per layer and the number of channels to 20, 40, 78, 78, 40, 20.

The planar baseline again uses 2D convolutions with 3×3 kernels and of channels to 18, 36, 72, 72, 36, 18 channels.

C.3 Input-output samples

We show extra examples of inputs and outputs for the dense prediction tasks. Figure 7 shows the vector field to image task while Fig. 8 shows the image to vector field task. Models are trained on the R mode, so they have access to rotated samples at training time. Nevertheless, the standard CNN and spherical CNN models are not equivariant in the vector field sense and cannot achieve the same accuracy as the SWSCNNs.

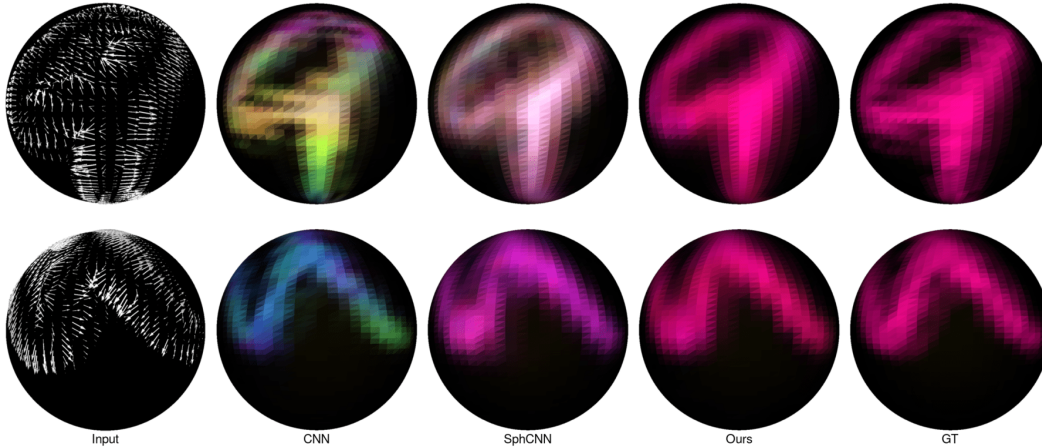


Figure 7: Input/output samples for the spherical vector field to image task. We show two rotated instances of the same input to highlight that standard CNNs and spherical CNNs do not respect the spherical vector field equivariance, while the SWSCNNs do.

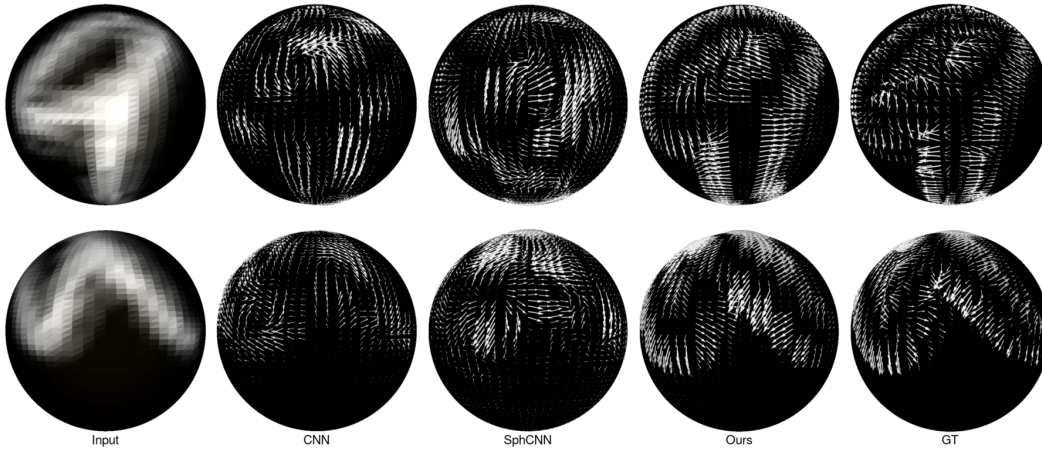


Figure 8: Input/output samples for the spherical image to vector field task.

D Spin-Weighted Spherical Harmonics Transforms

Our implementation of the SWSH decomposition and its inverse follows Huffenberger and Wandelt [21]. The basic idea is to leverage the relation between the SWSHs and the Wigner-D matrices. Recall that we can write the Wigner-D matrices as

$$D_{m,n}^{\ell}(\alpha, \beta, \gamma) = e^{-im\alpha} d_{m,n}^{\ell}(\beta) e^{-in\gamma}, \quad (18)$$

where d is a Wigner-d matrix.

We define $\Delta_{m,n}^{\ell}$ as

$$\Delta_{m,n}^{\ell} = d_{m,n}^{\ell}(\pi/2), \quad (19)$$

then the following relation holds [34],

$$d_{m,n}^\ell(\theta) = i^{m-n} \sum_{k=-\ell}^{\ell} \Delta_{k,m}^\ell e^{-ik\theta} \Delta_{k,n}^\ell. \quad (20)$$

Now we rewrite the SWSH forward transform,

$$\begin{aligned} {}_s\hat{f}_m^\ell &= \int_{\theta,\phi} {}_s f(\theta, \phi) \overline{{}_s Y_m^\ell(\theta, \phi)} \sin \theta \, d\theta \, d\phi \\ &= \int_{\theta,\phi} {}_s f(\theta, \phi) (-1)^s \sqrt{\frac{2\ell+1}{4\pi}} e^{is\psi} D_{m,-s}^\ell(\phi, \theta, \psi) \sin \theta \, d\theta \, d\phi \\ &= (-1)^s \sqrt{\frac{2\ell+1}{4\pi}} \int_{\theta,\phi} {}_s f(\theta, \phi) e^{-im\phi} d_{m,-s}^\ell(\theta) \sin \theta \, d\theta \, d\phi \\ &= (-1)^s \sqrt{\frac{2\ell+1}{4\pi}} \int_{\theta,\phi} {}_s f(\theta, \phi) e^{-im\phi} i^{m+s} \sum_{k=-\ell}^{\ell} \Delta_{k,m}^\ell e^{-ik\theta} \Delta_{k,-s}^\ell \sin \theta \, d\theta \, d\phi \\ &= (-1)^s i^{m+s} \sqrt{\frac{2\ell+1}{4\pi}} \sum_{k=-\ell}^{\ell} \Delta_{k,m}^\ell \Delta_{k,-s}^\ell \int_{\theta,\phi} {}_s f(\theta, \phi) e^{-im\phi} e^{-ik\theta} \sin \theta \, d\theta \, d\phi \\ &= (-1)^s i^{m+s} \sqrt{\frac{2\ell+1}{4\pi}} \sum_{k=-\ell}^{\ell} \Delta_{k,m}^\ell \Delta_{k,-s}^\ell I_{k,m}. \end{aligned}$$

Since the $\Delta_{m,n}^\ell$ are constants, they are pre-computed. We still need to compute

$$I_{k,m} = \int_{\theta,\phi} {}_s f(\theta, \phi) e^{-im\phi} e^{-ik\theta} \sin \theta \, d\theta \, d\phi, \quad (21)$$

which can be done efficiently with an FFT. There is a problem because ${}_s f$ is defined on the sphere so it is not periodic in both directions; we then define ${}_s f'$ as the periodic extension of ${}_s f$ which is a function on the torus. See McEwen [31] and Huffenberger and Wandelt [21] for more details about this extension. We can then express ${}_s f'$ by its Fourier coefficients,

$${}_s f'(\theta, \phi) = \sum_{p,q} {}_s \hat{f}'_{p,q} e^{ip\theta} e^{iq\phi}. \quad (22)$$

Substituting this in Eq. (21) yields,

$$\begin{aligned} I_{k,m} &= \int_{\theta=0}^{\pi} \int_{\phi=0}^{2\pi} \sum_{p,q} {}_s \hat{f}'_{p,q} e^{ip\theta} e^{iq\phi} e^{-im\phi} e^{-ik\theta} \sin \theta \, d\theta \, d\phi \\ &= \sum_{p,q} \int_{\theta=0}^{\pi} \int_{\phi=0}^{2\pi} {}_s \hat{f}'_{p,q} e^{i(p-k)\theta} e^{i(q-m)\phi} \sin \theta \, d\theta \, d\phi \\ &= \sum_p 2\pi \int_0^\pi {}_s \hat{f}'_{p,m} e^{i(p-k)\theta} \sin \theta \, d\theta \\ &= 2\pi \sum_p {}_s \hat{f}'_{p,m} \hat{w}(p-k), \end{aligned}$$

where \hat{w} can be obtained analytically. Note that the last expression is a 1D discrete convolution; if we see \hat{w} as the Fourier transform of some w , the convolution can be evaluated as the FFT of the

multiplication in the spatial domain,

$$I_{k,m} = \frac{2\pi}{N^2} \sum_{\theta,\phi} s f'(\theta, \phi) w(\theta) e^{-ik\theta} e^{-im\phi}, \quad (23)$$

for N uniformly sampled θ, ϕ . Here, w can be pre-computed, so the $I_{k,m}$ computation amounts to 1) extend the function to the torus, 2) apply the weights w , 3) compute a 2D FFT.